ORIGINAL PAPER

Kinetic and Stability Studies of Ru/La$_2$O$_3$ Used in the Dry Reforming of Methane

C. Carrara · J. Múnera · E. A. Lombardo ·
L. M. Cornaglia

Abstract The catalytic activity toward hydrogen production through the dry reforming of methane was determined for Ru supported on lanthanum oxide. The catalyst remained stable for more than 80 h in the 823–903 K temperature range and reactant partial pressure ratio (P_{CO_2}/P_{CH_4}) equal to unity. However, a significant deactivation was observed during the kinetic measurements when the catalyst was exposed to $P_{CO_2}/P_{CH_4} > 1$ at 823 K. In order to establish why the catalyst deactivated, the Ru reactivity in reductive and CO$_2$ rich atmospheres was studied by in situ LRS and XPS spectroscopies. The partial re-oxidation of metallic Ru could be one of the factors that produce the catalyst deactivation. To perform the kinetic measurements, the temperature range and the partial pressure ratios were selected within the window where the Ru catalyst was stable. The kinetic data and supporting spectroscopic evidence is consistent with a mechanism in which the metal and the oxide play key roles in decomposing the paraffin and activating the CO$_2$, respectively.

Keywords Kinetics · In situ LRS · Ru species

1 Introduction

One option to produce hydrogen fuel-cell grade from natural gas in one single vessel is through the use of a Pd membrane reactor [1]. The catalyst needed for this application must operate at temperatures below 873 K (ca.823 K) and should not produce carbonaceous residues. Otherwise, the membrane rapidly deteriorates. Noble metals like rhodium and ruthenium are more active than Ni for the dry reforming of methane. Furthermore, when the appropriate supports are used these formulations are catalytically stable and do not produce a significant amount of carbonaceous residues. As a bonus, ruthenium is much cheaper than rhodium. Several studies [2–5] have shown the high activity of Ru supported and exchanged catalysts. Bradford and Vannice [4] compared high dispersion catalysts (>50%) and found that the turnover frequencies decreased in the order TiO$_2$ > Alumina ≫ C. On the other hand, Wei and Iglesia [5] reported that forward turnover rates were strongly influenced by Ru dispersion but essentially insensitive to the identity of the support, although they did not use La$_2$O$_3$ as carrier. Our Ru–La based catalysts exhibit a forward reaction rate comparable to that previously reported by other authors [5] using different supports. The optimum Ru load on La$_2$O$_3$ was 0.6 wt% [6]. The role of La$_2$O$_3$ in the Rh and Ru lanthanum systems has been previously reported. In brief, lanthana helps to clean the catalyst surface by reacting with the carbon formed during the reforming of methane.

The activity and selectivity of Ru catalysts depend greatly on the oxidation state [7] of the metal, which can change depending on the reaction conditions and the support used. Laser Raman spectroscopy (LRS) combined with X-ray photoelectron spectroscopy (XPS) has been utilized to study the oxidation of ruthenium films at ambient pressure (1 atm) and temperatures between 298 and 573 K. The LRS probe provided in-situ vibrational information regarding surface oxide bonding, while XPS provided valuable complementary information on the metal and oxygen electronic states [8].

C. Carrara · J. Múnera · E. A. Lombardo · L. M. Cornaglia (✉)
Instituto de Investigaciones en Catálisis y Petroquímica (FIQ, UNL-CONICET), 2829-3000 Santiago del Estero, Santa Fe, Argentina
e-mail: lmcornag@fiq.unl.edu.ar

The goal of this study was to obtain a reliable kinetic equation for Ru/La$_2$O$_3$ catalysts and to study how temperature and CO$_2$ concentration affect the catalyst stability and the re-oxidation of metallic Ru employing in situ LRS and XPS spectroscopies.

2 Experimental

2.1 Catalyst Preparation

The Ru/La$_2$O$_3$ catalyst was prepared by the conventional wet impregnation of La$_2$O$_3$ (Anedra 99.99%) using RuCl$_3 \cdot$ 3H$_2$O. The resulting suspension was then heated at 353 K to evaporate the water and the solid material was dried in an oven at 383 K overnight. The catalysts were calcined for 6 h at 823 K in flowing air and then reduced at 823 K in H$_2$ flow for 2 h. The same preparation method was employed to obtain the Ru/SiO$_2$ sample. The weight percent of Ru is shown between parentheses.

2.2 Stability Tests

The catalyst (50 mg) was loaded into a tubular quartz reactor (inner diameter, 5 mm) which was placed in an electric oven. A thermocouple in a quartz sleeve was placed on top of the catalyst bed. The catalysts were heated in Ar at 823 K and then reduced in situ in flowing H$_2$ at the same temperature for 2 h. After reduction, the temperature was adjusted in flowing Ar to the reaction temperature, and the reactant gas mixture (P$_{CO_2}$:P$_{CH_4}$:P$_{Ar}$ = 1:1:1.1, P = 1 atm, W/F = 4.5 $\times$ 10^{-6} g h ml^{-1}) was fed to the reactor. The reaction products were analyzed in a TCD gas chromatograph (Shimadzu GC-8A) equipped with a Porapak column, and a molecular sieve column.

2.3 Kinetic Measurements

Kinetic studies under differential conditions were conducted in the same conventional flow system. The mass of catalyst used was 20–50 mg. This was diluted with 50 mg of inert powder quartz to avoid temperature gradients. Prior to reaction, the catalyst was heated in Ar to 823 K and then reduced in situ at the same temperature in a H$_2$ flow for 2 h. Conversions were usually controlled to be significantly lower ($\leq$6%) than those defined by thermodynamic equilibrium by adjusting the total flow rate (187 mL/min) and varying the partial pressures of CH$_4$ (P$_{CH_4}$) and CO$_2$ (P$_{CO_2}$). Rate limitation by external and/or internal mass transfer under differential conditions proved to be negligible by applying suitable experimental criteria.

2.4 Catalyst Characterization

2.4.1 Metal Dispersion

The Ru dispersion of the fresh catalyst, following the hydrogen reduction at 823 K for 2 h was determined by static equilibrium adsorption of H$_2$ or CO at 373 K in a conventional vacuum system.

2.4.2 X-Ray Photoelectron Spectroscopy (XPS)

XPS analyses were performed in a multi-technique system (SPECS) equipped with a dual Mg/Al X-ray source and a hemispherical PHOIBOS 150 analyzer operating in the fixed analyzer transmission (FAT) mode. The spectra were obtained with pass energy of 30 eV; an Mg-Kα X-ray source was operated at 100 W and 10 kV. The working pressure in the analyzing chamber was less than 5 $\times$ 10^{-9} mbar. The XPS analyses were performed on the used catalyst and on the calcined solid after different treatments carried out in the reaction chamber of the spectrometer. The samples were heated up in flowing H$_2$/Ar or CO$_2$/Ar mixtures at 723 K. The spectral regions corresponding to La 3d, O 1s, C 1s, Ru 3d, and Ru 3p core levels were recorded for each sample. The data treatment was performed with the Casa XPS program (Casa Software Ltd, UK). The peak areas were determined by integration employing a Shirley-type background. Peaks were considered to be a mixture of Gaussian and Lorentzian functions in a 70/30 ratio. For the quantification of the elements, sensitivity factors provided by the manufacturers were used.

2.4.3 Laser Raman Spectroscopy (LRS)

The Raman spectra were recorded with a TRS-600-SZ-P Jasco Laser Raman instrument, equipped with a CCD (charge coupled device) with the detector cooled to about 153 K using liquid N$_2$. The excitation source was the 514.5 nm line of a Spectra 9000 Photometrics Ar ion laser. The laser power was set at 30 mW.

In situ Raman catalyst characterization experiments were performed using a Raman cell. The Raman spectra were taken from room temperature to 573 K under a reductive atmosphere (10% H$_2$ in Ar mixture). The laser beam was focused on the top of the catalyst bed and the cell was heated at 5 K/min. After 5 min at 573 K, the gas flow was switched to a CO$_2$/Ar (30%) mixture increasing temperature to 773 K, and the Raman spectra were measured at several temperatures. At 773 K, the spectra were recorded at different exposure times. Then, the catalyst bed was exposed to an Ar flow from 773 K to room temperature and the Raman spectrum was obtained at 298 K. All the spectra were recorded under steady-state conditions.

3 Results and Discussion

3.1 Stability Tests

The catalyst stability experiments were performed at 823 and 903 K in a fixed-bed reactor. Figure 1 shows CH_4 and CO_2 conversions versus time. They are significantly lower than thermodynamic equilibrium values. The solid remained stable for more than 80 h in the 823–903 K temperature range and $P_{CO_2}/P_{CH_4} = 1$. The CO_2 conversion was higher than the CH_4 conversion due to the occurrence of the RWGS reaction in which CO_2 reacted with the H_2 produced in the reforming reaction; this is consistent with a H_2/CO ratio lower than unity (not shown).

The stoichiometry of these reactions demands that

$$H_2/CO = (3 - x_{CO_2}/x_{CH_4})/(1 + x_{CO_2}/x_{CH_4})$$

where x_{CH_4} and x_{CO_2} are the experimental CH_4 and CO_2 conversions, respectively [4]. This ratio was satisfied for all the measured points.
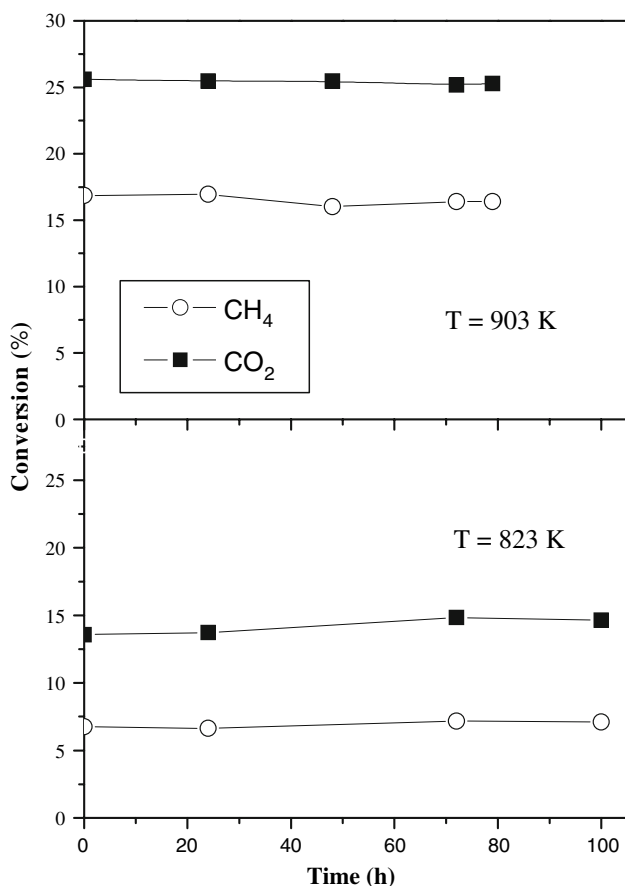

Fig. 1 Stability tests in a fixed-bed reactor at 823 and 903 K. (P_{CO_2}:P_{CH_4}:P_{Ar} = 1:1:1.1, W/F = 4.5×10^{-6} g h mL^{-1})

3.2 Influence of Temperature and P_{CO_2}/P_{CH_4} Ratio on the Catalyst Stability

The first set of kinetic measurements was performed with $P_{CO_2} = P_{CH_4} = 40$ kPa and then one of the reactant partial pressures (P_{CO_2} or P_{CH_4}) was decreased. After finishing the complete range, the measurements were repeated employing a P_{CO_2}/P_{CH_4} ratio equal to 1, in order to obtain duplicate values and verify the catalyst stability during the kinetic study. The results are shown in Fig. 2a. When the catalyst was exposed to a $P_{CO_2}/P_{CH_4} > 1$ at 823 K, the duplicate experiments showed an irreversible deactivation of the solid whereas the same solid was stable at this temperature employing $P_{CO_2}/P_{CH_4} = 1$ (Fig. 1). Therefore, the kinetic measurements varying the P_{CH_4} were carried out at $P_{CO_2} = 10$ kPa.

When the measurements were carried out keeping constant the $P_{CO_2} = 10$ kPa and varying the P_{CH_4} between 5 and 40 kPa, a significant catalyst deactivation was observed at 903 K (Fig. 2b). However, when the $P_{CO_2}/P_{CH_4} = 1$, the catalyst was stable for 80 h at this temperature (Fig. 1).

Several possible causes for Ru-catalyst deactivation could be proposed, such as carbon deposition on the catalyst surface or increase of Ru particles size as well [9]. In order to establish why the catalyst deactivated, the Ru reactivity in reductive and CO_2 rich atmospheres was studied by in situ LRS and XPS spectroscopies.
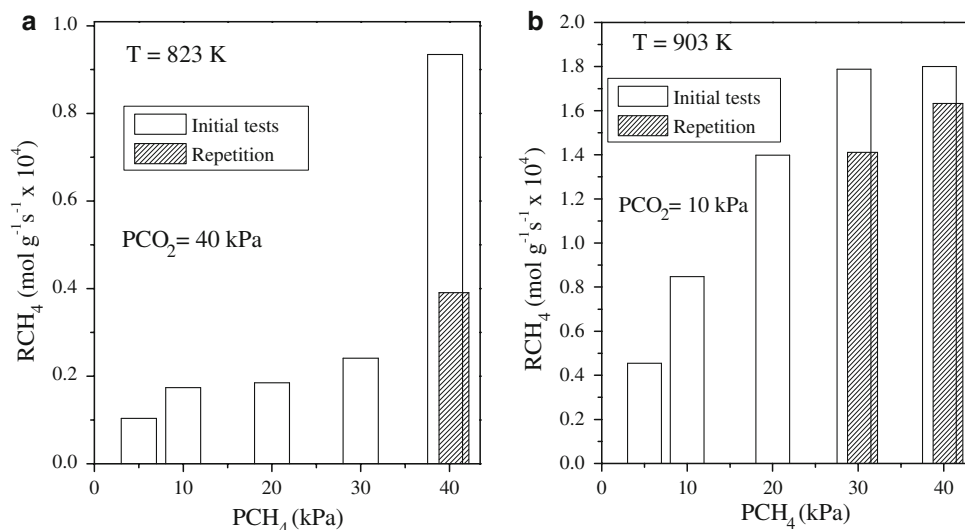
3.3 Reactivity of Ru and La Species

The XRD patterns for the calcined catalyst showed the presence of II-$La_2O_2CO_3$ and $La(OH)_3$ phases. For the used catalysts, only II-$La_2O_2CO_3$ was observed. No XRD reflections associated with Ru compounds were detected in any case [6].

LRS has been used to study the oxidation of ruthenium films at atmospheric pressure [8]. RuO_2, RuO_4, and RuO_3 have been detected upon thermal oxidation of initially reduced Ru surface. However, only a few papers have reported the application of this technique to characterize Ru supported catalysts [10].

We have recently [6] employed LRS to characterize the Ru-lanthanum system. The Raman spectra of the Ru/La_2O_3 catalysts calcined at 823 K exhibited peaks at 358, 384, 747, and 1086 cm^{-1}, previously assigned [11] to the hexagonal form of the lanthanum oxycarbonate (II-$La_2O_2CO_3$). The broad Raman band at 670 cm^{-1} was attributed to Ru(III) that strongly interacts with La.

Yan et al. [10] studied Ru/SiO_2 and Rh/SiO_2 catalysts during the partial oxidation of methane using LRS. They found that the Raman spectrum recorded at 600 °C under O_2 showed two bands (at 489 and 609 cm^{-1}) attributable to
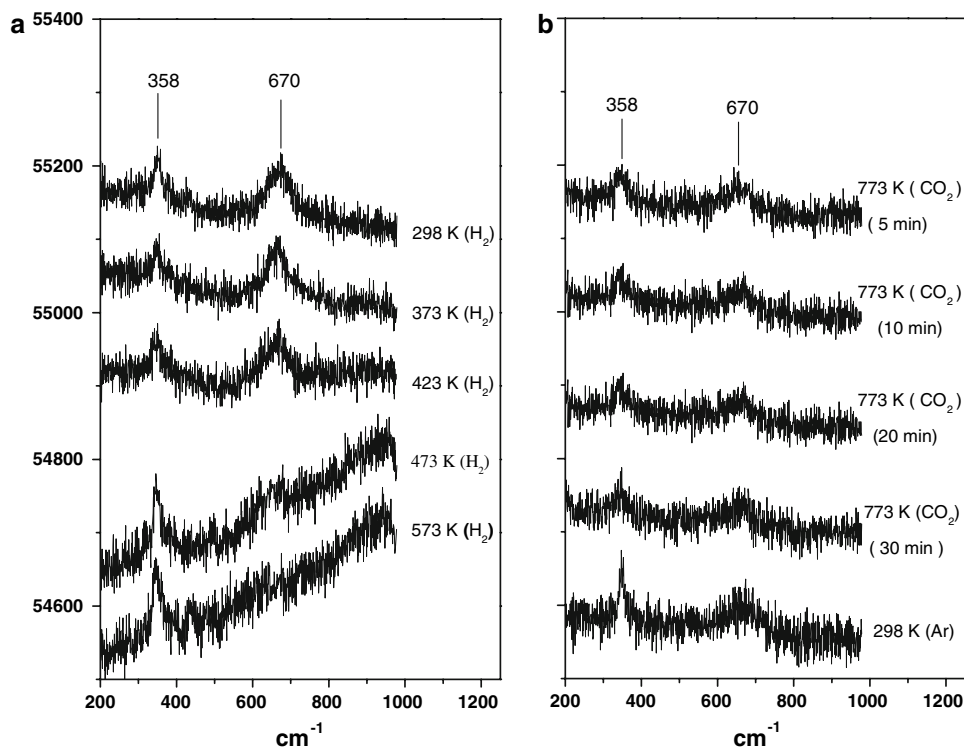
RuO$_2$. These bands vanished under H$_2$ flow and reappeared when a CH$_4$/O$_2$/Ar stream was switched on at the same temperature.

To study the reactivity of Ru species in H$_2$ and CO$_2$ rich atmospheres, in situ Raman experiments were performed. The Raman spectra of the Ru/La$_2$O$_3$ catalyst during in situ reduction are shown in Fig. 3a. The spectra exhibit a peak at 358 cm^{-1} previously assigned to lanthanum oxycarbonate (II-La$_2$O$_2$CO$_3$) and a broad band at 670 cm^{-1} related to Ru(III) strongly interacting with La. When the temperature was increased up to 473 K, this band disappeared, suggesting the reduction of the Ru species [6].

The TPR profile for our Ru/La$_2$O$_3$ solid [6] showed a main reduction peak at 533 K and a second one at 648 K. The peak at 533 K was assigned to the presence of a strong metal-support interaction. These results are in agreement with the reduction experiments performed in the Raman cell, no Ru Raman peaks being observed after reduction at 573 K (Fig. 3a).

After reduction, a 30% CO$_2$/Ar mixture was fed to the Raman cell and the temperature was increased from 573 to 773 K. The 358 cm^{-1} intensity band increased and the broad band at 670 cm^{-1} was detected, increasing with the CO$_2$ exposure time (Fig. 3b). These results suggest the

Fig. 3 In situ Laser Raman spectra of calcined Ru(0.6)/
La$_2$O$_3$ catalyst exposed to **a** flowing H$_2$ **b** flowing CO$_2$

re-oxidation of Ru^0. Then, the catalyst was exposed to an Ar flow (≈ 30 mL/min) from 773 to 298 K; the Raman spectrum taken at room temperature confirms the previous observation.

The Ru re-oxidation is consistent with the observation of Yan et al. [10]. They reported a significant catalytic difference between Rh/SiO_2 and Ru/SiO_2 which was attributed to the great differences in the Rh–O (405.0 kJ/mol) and Ru–O (528.4 kJ/mol) bond strengths. This renders the reduction of Ru/SiO_2 more difficult than that for Rh/SiO_2. For the Rh/La_2O_3 system, we did not observe any deactivation at high P_{CO_2}/P_{CH_4} ratio (oxidant conditions).

3.4 Surface Ru Species

The XPS measurements were performed on samples treated in an atmospheric pressure (1 atm) reactor attached to the spectrometer. The samples could be transferred to the UHV chamber for spectral acquisition without exposure to air. The surface reduction and oxidation were undertaken in a similar way to the LRS experiments.

The effects of reduction at 723 K on the main core level peaks are presented in Fig. 4 and in Tables 1 and 2 that summarize the intensity ratios and binding energies (BE). Figure 4 shows the Ru 3d spectra obtained on the Ru catalyst after reduction and CO_2 treatment at 723 K performed in the chamber attached to the spectrometer. There is an overlap between Ru 3d and C 1s peak at 284.8 eV. The latter peak that corresponds to the contamination carbon taken as reference was subtracted from the original spectrum. Also, the C 1s spectra exhibit a well defined peak at 289.3 eV that was attributed to carbonate carbon [12].

For the calcined solids, two Ru $3d_{5/2}$ peaks could be observed at 282.7 and 284.0 eV (Table 1). According to the literature, these high binding energy values indicate the presence of Ru^{n+} species [13]. The binding energy of 284.0 eV measured in Ru/Al_2O_3 by several authors [13, 14] was attributed to Ru (IV) species deposited onto the alumina surface.

The Ru state with a BE of 282 eV is known from the literature and has been assigned [14] to Ru(IV)/Ru(III) oxyhydrates, Ru^{+2} on Al_2O_3, and Ru^+ in Y zeolite. Elmasides et al. [14] assigned this BE to an intermediate Ru oxidation state, most likely Ru(II). This state appeared to be stable on Al_2O_3. They found that on alumina, ruthenium is incompletely reduced by treatment with H_2 at 823 K while on TiO_2, Ru is more easily reduced to the metallic state. They found that the chemical behavior depends strongly on the material on which it is supported.

For the mixed $LaRu_{1-x}Ni_xO_3$ perovskite-type oxides, two well-defined peaks of Ru $3d_{5/2}$, one at ≈ 280 eV attributed to Ru^0 and a second one at ≈ 282.6 eV
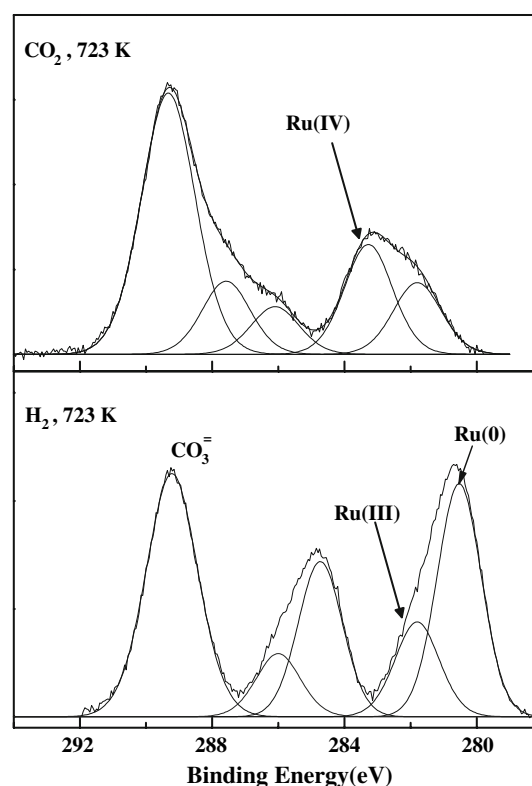

Fig. 4 C 1s–Ru 3d XPS region for $Ru(0.6)/La_2O_3$ after different treatments in the reaction chamber

corresponding to unreduced Ru (Ru(III)) were reported by Goldwaser [15]. For the most active perovskite (LaRu$_{0.8}$Ni$_{0.2}$O$_3$), the signal attributed to Ru(III) appeared at 281.7 eV indicating the existence of a different Ru species in this solid attributed to partially reduced Ru. In our case, we have previously assigned [6] the 282 eV peak of calcined Ru/La_2O_3 solids to Ru(III).

After reduction of $Ru(0.6)/La_2O_3$, there appeared a peak at 280.2 eV (Fig. 4) that corresponds to Ru^0. The peak at 281.8 eV was still present but in low proportions. The Ru 3p peak was also analyzed due to the overlapping of C 1s and Ru 3d contributions. Figure 5 shows the Ru $3p_{3/2}$ spectra for both the calcined and reduced $Ru(0.6)/La_2O_3$ sample. A shift to 462.3 eV in the reduced solid with respect to that at 463.8 eV in the calcined sample may be observed. This change confirms the surface reduction to Ru^0 upon treatment with hydrogen [16].

The position of the La 3d peaks shifts to lower binding energies and the satellite-split slightly increases. The O 1s spectra invariably show two peaks: one at 531.2 eV assigned to the carbonate and hydroxyl species, and another at 528.8 eV corresponding to lattice oxygen $O^=$ [17]. Following reduction at 723 K, the higher binding energy peak decreases in intensity and the second one becomes well-defined. Their relative intensities are shown in Table 1.

Table 1 Binding energies[a] (BE) of the Ru(0.6)/La$_2$O$_3$ solid after different treatments

Treatment	Ru 3d$_{5/2}$	C 1s CO$_3^=$(eV)	O 1s		Ru 3p$_{3/2}$	La 3d
			BE(eV)	%[b]		
Calcined	282.7 (2.1)[c]	289.3 (1.9)	531	89	463.6(4.3)	834.6 (3.1)
	284.0 (2.1)		528.4	11		[3.5][c]
Reduced at 723 K	280.5 (1.6)	289.2 (1.8)	531.1	57	462.3(4)	833.6 (2.7)
	281.8 (1.6)		528.5	43		[4.0]
CO$_2$ at 723 K	281.8 (1.7)	289.3 (1.9)	531.8	69	463.9(4.4)	834.1 (2.8)
	283.2 (1.7)		528.7	31		[3.8]
Used at 903 K	280.0 (1.8)	289.3 (1.8)	531.1	71	461.5(4.3)	834.1 (3.0)
	281.1 (1.8)		528.5	29		[3.6]

[a] The C 1s at 284.8 eV was taken as reference

[b] The relative % of oxygen species

[c] The FWHM (eV) are given between parentheses and the satellite-split between brackets

Table 2 Surface atomic ratios of the Ru(0.6)/La$_2$O$_3$ solid after different treatments

Treatment[a]	Ru 3d$_{5/2}$/La	Ru 3p$_{3/2}$/La	O/La	CCO$_3^=$/La	CCO$_3^=$/O531.1	Ru(at%)[b]
Calcined	0.10	0.12	3.7	0.65	0.19	1.8
Reduced at 723 K	0.044	0.044	2.1	0.31	0.34	1.3
CO$_2$ at 723 K	0.049	0.06	2.8	0.60	0.31	1.1
Used at 823 K[c,d]	0.12	–	3.8	0.89	0.24	2.0
Used at 903 K[c]	0.069	0.067	3.7	0.54	0.20	1.3

[a] Ru/La nominal = 0.0096

[b] Surface atomic Ru concentration

[c] Samples exposed to air after the kinetic measurements

[d] From Faroldi et al. [6]

The measured surface Ru/La ratio for the calcined Ru solid is higher than the nominal ratio (Ru/La = 0.0096). However, after treatments a significant decrease is observed (Table 2). The O/La and CCO$_3^=$/La decrease from 3.7 and 0.65 for the calcined solid to 2.1 and 0.31 for the solid reduced in flowing H$_2$/Ar mixture in the reaction chamber of the spectrometer at 723 K. The O/La ratios show high values suggesting the presence of surface OH. Also, after reduction the CCO$_3^=$/O531.1 ratio agrees well with the stoichiometric value for surface CO$_3^=$.

After the measurements of the reduced sample, the instrument reaction chamber was fed with a flowing 30% CO$_2$/Ar mixture, and the temperature was increased to 723 K and kept constant during 30 min. Then, the sample was cooled down, degassed and introduced into the main chamber for the spectra acquisition. The recorded Ru 3d spectrum is shown in Fig. 4. In this case, Ru appears mainly as Ru(IV) with a low concentration of Ru(III), indicating a surface re-oxidation after CO$_2$ treatment.

Our in situ LRS and XPS data suggest that the partial re-oxidation of metallic Ru could be one of the factors that produce the catalyst deactivation in rich CO$_2$ streams. This effect could be more pronounced at T > 873 K.

3.5 La-Ru Species and Carbon Deposits on Used Samples

The XRD and Raman data of the used catalysts indicated that only type II oxycarbonate was present. The Raman peak at 670 cm^{-1} almost vanished [6], in agreement with the reduced state of the sample. Also, a group of very low intensity and broad Raman bands at 1,340 and 1,590 cm^{-1} was observed, assigned to graphitic carbon [11]. However, for all the used catalysts reported in the present paper, no carbon deposition was detected through TGA measurements. The tiny amount of carbon deposits did not significantly affect the activity in the differential reactor. This behavior could be related to the sites on which carbon is deposited and/or to the role of reaction intermediate that the carbon would play.

For the used catalysts, the XPS Ru/La atomic ratio slightly changed compared to the calcined sample (Table 2), suggesting that no change in the ruthenium dispersion has occurred at 823 K. After being used at 903 K, Ru(0) and Ru(III) surface species were observed (Fig. 6). Also, the Ru/La atomic ratio decreased, at high temperature. This may indicate that the state of the used
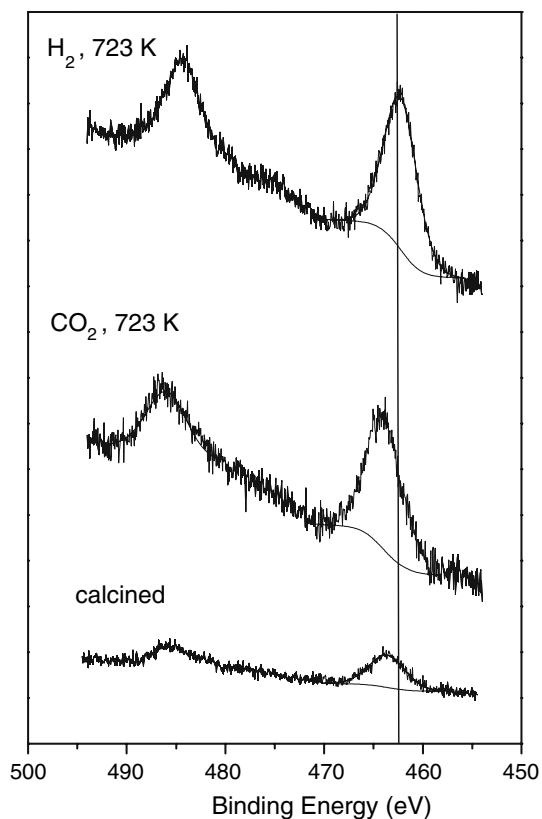
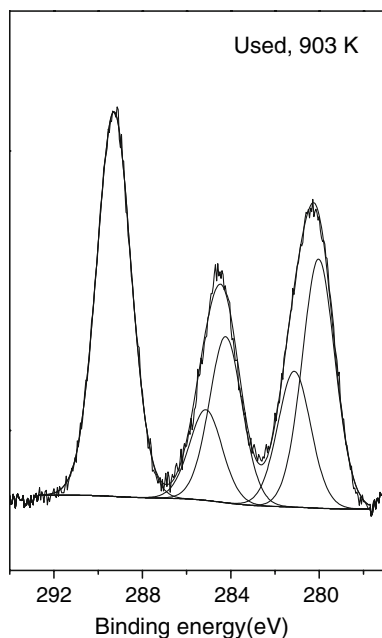**Fig. 5** Ru 3p spectra for Ru(0.6)/La$_2$O$_3$ after different treatments

Fig. 6 C 1s–Ru 3d XPS region for Ru(0.6)/La$_2$O$_3$ after the stability test at 903 K

catalyst results from a Ru re-oxidation and reduction cycles, in the course of which it becomes aggregated [14]. The oxidation of Ru/La$_2$O$_3$ catalysts in CO$_2$ pulses was

also reported by Matsui et al. [7]. They studied the effect of support on the activities and mechanisms in the CO$_2$ reforming of methane over Ru catalysts. Over Ru/La$_2$O$_3$ catalysts they proposed the following reaction step based on pulse experiments

$$Ru/La_2O_3 + CO_2(ad) \Rightarrow CO(gas) + Ru - Ox/La_2O_3$$

3.6 Kinetic Measurements

The temperature range and the partial pressure ratios were selected within the window where the Ru catalyst was stable. Figure 7 shows the influence of these variables on the rate of methane consumption. These studies were performed at atmospheric pressure in the temperature range of 783–863 K under differential conditions. The measurements were made maintaining the partial pressure of one reactant constant: $P_{CH_4} = 40\,kPa$ (Fig. 7a) or $P_{CO_2} = 10\,kPa$ (Fig. 7b) and varying the pressure of the other reactant between 5 and 40 kPa. It is shown that the reaction rate is strongly affected by $P_{CO_2} < 20\,kPa$ at $P_{CH_4} = 40\,kPa$, while the influence is very strong in the whole pressure range when $P_{CO_2} = 10\,kPa$.

The reaction rates have not been normalized per metal atom due to uncertainties in determining the metal surface area in the presence of the decorating support. A dispersion value lower than 5% was obtained from CO and H$_2$ chemisorption results. The low chemisorption after a high temperature reduction is probably not indicative of the real dispersion due to the occurrence of a strong interaction between the metal and the support [12, 18].

In order to check the differential conditions, the forward reaction rates (r_f) were calculated from the net rate of reaction (r_n). The r_f can be estimated as follows: [5, 19]
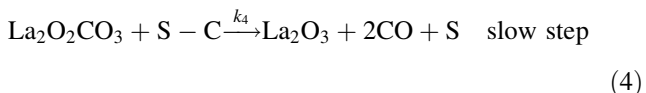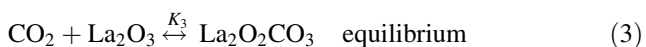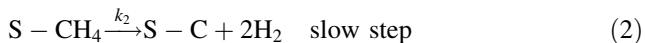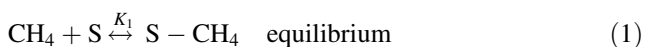
$$r_f = r_n(1 - \eta)$$
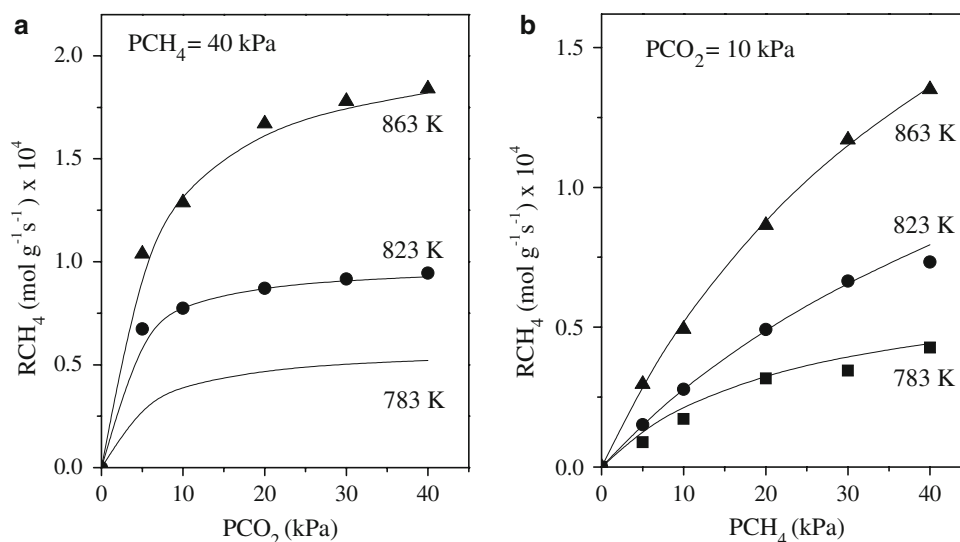
$$\eta = \frac{(P_{CO})^2(P_{H_2})^2}{P_{CH_4}P_{CO_2}} \frac{1}{Ke}$$

where P_is are the prevalent pressures of reactants and products and Ke is the equilibrium constant calculated at the corresponding reaction temperature. The calculated η values were lower than 0.0025 confirming the quality of the differential data obtained.

3.7 Kinetic Model

As the support participates actively in the reaction mechanism, we adopted the mechanism proposed by Verykios et al. [20] for Ni/La$_2$O$_3$ and already successfully applied by Múnera et al. [21, 22] for Rh/La$_2$O$_3$ and Rh/La$_2$O$_3$–SiO$_2$.

Fig. 7 Fit of the proposed kinetic model for the CO_2 reforming of methane. Curves were calculated using Eq. 5

the other reactant constant at each temperature. Using these values our data are correctly fit (Fig. 7a and b).

Our model allows the calculation of K_1, k_2, and the K_3k_4 product. In order to decouple this product, the thermodynamic data for calculating the K_3 values were obtained from Shirsat et al. [23] as indicated in Table 3.

The temperature dependence of k_i and K_i is shown in the following equations:

$$CH_4 + S \overset{K_1}{\leftrightarrow} S - CH_4 \quad \text{equilibrium} \tag{1}$$

$$S - CH_4 \overset{k_2}{\longrightarrow} S - C + 2H_2 \quad \text{slow step} \tag{2}$$

$$CO_2 + La_2O_3 \overset{K_3}{\leftrightarrow} La_2O_2CO_3 \quad \text{equilibrium} \tag{3}$$

$$La_2O_2CO_3 + S - C \overset{k_4}{\longrightarrow} La_2O_3 + 2CO + S \quad \text{slow step} \tag{4}$$

$$r_{CH_4} = \frac{K_1k_2K_3k_4[CH_4][CO_2]}{K_1K_3k_4[CH_4][CO_2] + K_1k_2[CH_4] + K_3k_4[CO_2]} \tag{5}$$

The rate equation (Eq. 5) was derived assuming that steps (2) and (4) are the slow ones and that the surface coverage by adsorbed H_2 and CO is negligible. The effective rate constant values summarized in Table 3 were calculated from the linear plots $1/r_{CH_4}$ vs. $1/P_i$, where (i) correspond to either CO_2 or CH_4 keeping the pressure of

$$K_1 = 1.46 \times 10^{-6} \times \exp(+7242/T) [kPa^{-1}] \tag{6}$$

$$k_2 = 2.94 \times 10^3 \times \exp(-12949/T) [mol/g\,s], \tag{7}$$

$$K_3 = 4.05 \times 10^8 \times \exp(+15891/T) [(mol/g\,s)(kPa^{-1})] \tag{8}$$

$$k_4 = 2.04 \times 10^8 \times \exp(-26226/T) [mol/g\,s] \tag{9}$$

Note that both the methane adsorption enthalpy (−14.4 kcal/mol) and entropy are negative, in this way

Table 3 Kinetic model parameters for Ru(0.6)/La$_2$O$_3$

Parameters	Temperatures		
	783 K	823 K	863 K
K_1[a,b]	$(1.62 \pm 0.14) \times 10^{-2}$	$(8.48 \pm 1.10) \times 10^{-3}$	$(6.92 \pm 0.91) \times 10^{-3}$
k_2[a,c]	$(2.03 \pm 0.41) \times 10^{-4}$	$(3.88 \pm 0.54) \times 10^{-4}$	$(9.45 \pm 1.21) \times 10^{-4}$
K_3k_4[a,d]	$(1.31 \pm 0.12) \times 10^{-5}$	$(4.16 \pm 0.36) \times 10^{-5}$	$(4.07 \pm 0.62) \times 10^{-5}$
K_3[a,e]	26.41 ± 0.22	10.02 ± 0.11	3.74 ± 0.02
K_4[f]	$(4.95 \pm 0.61) \times 10^{-7}$	$(4.08 \pm 0.23) \times 10^{-6}$	$(1.09 \pm 0.07) \times 10^{-5}$

[a] Values are reported ±95% confidence interval (5 data points for each linear regression)

[b] Equilibrium constant of methane adsorption [kPa^{-1}]

[c] Rate constant of the decomposition of methane [mol g^{-1} s^{-1}]

[d] Product of the equilibrium constant of the reaction between CO_2 and La_2O_3 and the rate constant of reaction between the oxycarbonate species and carbon deposited on the surface of Ru [mol g^{-1} s^{-1} kPa^{-1}]

[e] From Shirsat et al.[23] [kPa^{-1}]

[f] Rate constant of the reaction between the oxycarbonate species and carbon formed on the catalyst surface [mol g^{-1} s^{-1}]
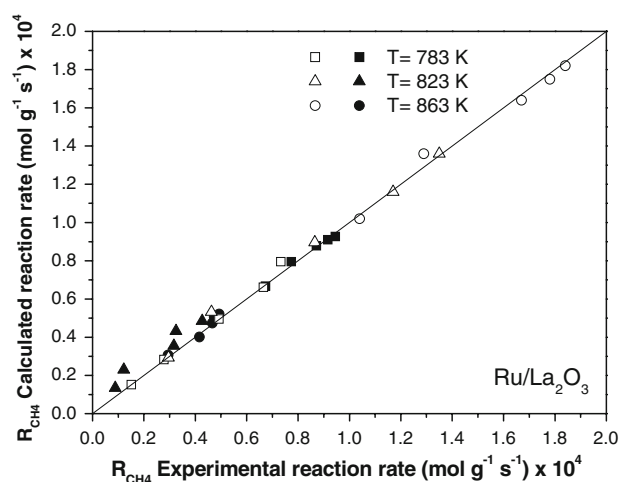
Fig. 8 Parity plot. The data was obtained maintaining either P_{CO_2} (full symbols) or P_{CH_4} (empty symbols) constant

lending additional credibility to the mechanistic model and the assumptions made in deriving the kinetic equation (Eq. 5).

The parity plot (Fig. 8) shows a very good correlation between the calculated and experimental reaction rates obtained at different temperatures.

The best reference data on Ru and Rh supported catalysts were reported by Wei and Iglesia [5, 19]. They obtained an activation energy of 26.6 kcal/mol for methane disappearance when they used Rh(0.4%)/Al$_2$O$_3$ as the catalyst. This is very close to ours of 24.8 kcal/mol obtained by adding the values derived from the corresponding Eqs. 6 and 7 for the Rh(0.6)/La$_2$O$_3$ solid [21]. Wei and Iglesia [19] also measured this parameter for the Ru(3.2%)/Al$_2$O$_3$ solid (22.9 Kcal/mol); however, this value is not similar to ours for Ru(0.6)/La$_2$O$_3$ (11.4 kcal/mol). Note that on Al$_2$O$_3$, the adsorption of CO$_2$ is negligible and consequently they found a first order dependency of the reaction rate on methane partial pressure and zero order on carbon dioxide.

4 Conclusions

– In situ LRS and XPS data suggest that the partial re-oxidation of metallic Ru could be one of the factors that lead to catalyst deactivation in rich CO$_2$ streams.

– The XPS Ru/La atomic ratio decreased after kinetic measurements at high temperature. This may indicate that the state of the used catalyst results from Ru re-oxidation and reduction cycles, in the course of which it becomes aggregated.

– The kinetic data and supporting spectroscopic evidence is consistent with a mechanism in which the metal and the oxide play key roles in decomposing the paraffin and activating the CO$_2$, respectively.

– The reaction mechanism previously applied to other lanthanum based catalysts fits well with the kinetic behavior of the Ru formulation.

References

1. Irusta S, Múnera J, Carrara C, Lombardo EA, Cornaglia LM (2005) Appl Catal A 287:147
2. Portugal UL, Marques CM, Araujo EC, Morales EV, Giotto MV, Bueno JMC (2000) Appl Catal A Gen 193:173
3. Ferreira-Aparicio P, Rodriguez-Ramos L, Anderson JA, Guerrero-Ruiz A (2000) Appl Catal A Gen 202:183
4. Bradford M, Vannice MA (1999) J Catal 183:69
5. Wei J, Iglesia E (2004) J Phys Chem B 108:7253
6. Faroldi B, Carrara C, Lombardo EA, Cornaglia LM (2007) Appl Catal A 319:38
7. Matsui N, Anzai K, Akamatsu N, Nakagawa K, Ikenaga N, Suzuki T (1999) Appl Catal A 179:247
8. Chan H, Takoudis CG, Weaver MJ (1997) J Catal 172:336
9. Bradford M, Vannice M (1999) Catal Rev Sci Eng 41:1
10. Yan GG, Wu T, Weng W, Toghiani H, Toghiani RK, Wan HL, Pittman CU (2004) J Catal 226:247
11. Cornaglia L, Múnera J, Irusta S, Lombardo E (2004) Appl Catal A Gen 263:91
12. Gallaher G, Goodwin J, Huang C, Houalla M (1993) J Catal 140:453
13. Tsisum E, Nefedov B, Shpiro E, Antoshin G, Minachev K (1984) React Kinet Catal Lett 24:37
14. Elmasides C, Kondarides DI, Grünert W, Verykios XE (1999) J Phys Chem B 103:5227
15. Goldwasser MR, Rivas ME, Pietri E, P′erez-Zurita MJ, Cubeiro ML, Grivobal-Constant A, Leclercq Goldwaser G (2005) J Mol Catal A Chem 228:325–331
16. Navarro RM, Alvarez-Galvan MC, Villoria JA, Gonzalez-Jimenez ID, Rosa F, Fierro JLG (2007) Appl Catal B 73:247–258
17. Lacombe S, Geantet C, Mirodatos C (1994) J Catal 151:439
18. Chan S, Bell A (1984) J Catal 89:433
19. Wei J, Iglesia E (2004) J Catal 225:116
20. Verykios X (2003) Int J Hydrogen Energy 28:1045
21. Múnera JF, Irusta S, Cornaglia LM, Lombardo EA, Vargas César D, Schmal M (2006) J Catal 245:25
22. Múnera JF, Cornaglia LM, Vargas César D, Schmal M, Lombardo EA (2007) Ind Eng Chem Res 46:7543
23. Shirsat AN, Ali M, Kaimal KN, Bharadwaj SR, Das D (2003) Thermochim Acta 399:167